The Astrophysical Journal, 764:134 (5pp), 2013 February 20 doi:10.1088/0004-637X/764/2/134

NEW CLASS OF VERY HIGH ENERGY γ-RAY EMITTERS: RADIO-DARK MINI SHELLS SURROUNDING ACTIVE GALACTIC NUCLEUS JETS

Motoki Kino[1], Hirotaka Ito[2], Nozomu Kawakatu[3], and Monica Orienti[4,5]
[1] ISAS/JAXA, 3-1-1 Yoshinodai, 229-8510 Sagamihara, Japan; kino@vsop.isas.jaxa.jp
[2] Yukawa Institute for Theoretical Physics, Kyoto University, Oiwake-cho Kitashirakawa Sakyo-ku, Kyoto 606-8502, Japan
[3] Graduate School of Pure and Applied Sciences, University of Tsukuba, 1-1-1 Tennodai, Tsukuba 305-8571, Japan
[4] Dipartimento di Astronomia, Universita di Bologna, via Ranzani 1, I-40127 Bologna, Italy
[5] INAF-Istituto di Radioastronomia, via Gobetti 101, I-40129 Bologna, Italy
Received 2012 September 4; accepted 2012 December 27; published 2013 January 31

ABSTRACT

We explore non-thermal emission from a shocked interstellar medium, which is identified as an expanding shell, driven by a relativistic jet in active galactic nuclei (AGNs). In this work, we particularly focus on parsec-scale size mini shells surrounding mini radio lobes. From the radio to X-ray band, the mini radio lobe emission dominates the faint emission from the mini shell. On the other hand, we find that inverse-Compton (IC) emission from the shell can overwhelm the associated lobe emission at the very high energy (VHE; $E > 100\,\mathrm{GeV}$) γ-ray range, because energy densities of synchrotron photons from the lobe and/or soft photons from the AGN nucleus are large and IC scattering works effectively. The predicted IC emission from nearby mini shells can be detected with the Cherenkov Telescope Array and they are potentially a new class of VHE γ-ray emitters.

Key words: galaxies: active – galaxies: jets – gamma rays: galaxies – radiation mechanisms: non-thermal – radio continuum: galaxies

Online-only material: color figures

1. INTRODUCTION

Radio-loud active galactic nuclei (AGNs) are among the most powerful objects in the universe. According to the standard picture of jets in AGNs, the jets are enveloped in a cocoon consisting of shocked jet material and the cocoon is surrounded by shocked interstellar medium. The shocked ambient region (hereafter we refer to as the shell) is identical to the forward shocked region and it is a fundamental ingredient in the whole AGN jet system. Despite this, physical properties of shells have not been well studied since they are not bright and remain undetected except for thermal X-ray detections of shells surrounding bubbles in Centaurus A (Croston et al. 2009), NGC 3801 (Croston et al. 2007), and in the Galactic center (Su et al. 2010 and references therein). In the radio band, shells are dim (Carilli et al. 1988) and their overall emissions are overwhelmed by the radio bubbles (radio lobes) identical to a portion of the cocoon.

Recently, we indicated a possibility of very high energy (VHE) γ-ray emissions from AGN shells in Ito et al. (2011, hereafter I11). In I11, the non-thermal emission of a shell is mainly produced by inverse-Compton (IC) mechanism for compact sources (less than $\sim$10 kpc), while synchrotron radiation is more important for larger shells. Physical properties of nearby shells can be proved by the detection of IC emissions using modern Cherenkov telescopes. The examined shell size in I11 was, however, limited to 1–100 kpc. In this paper, we complement the work of I11 by exploring smaller shells. I11 indicate that smaller shells may be a new class of VHE γ-ray emitters in the universe and in the present work we quantitatively examine the theoretically predicted photon spectra from the mini shells. To clarify the detection feasibility by the next-generation instrument Cherenkov Telescope Array (CTA), we further examine the non-thermal emission on 10 pc scale, which corresponds to the smallest scale of radio bubbles ever observed, properly taking into account the $\gamma\gamma$ absorption by extragalactic background light (EBL). The CTA will consist of two arrays of Cherenkov telescopes, which aim to: (1) increase sensitivity by one order of magnitude for deep observations around 1 TeV, (2) significantly boost the detection area and hence detection rates, (3) increase the angular resolution and hence the ability to resolve the morphology of extended sources, (4) provide uniform energy coverage for photons from some tens of GeV to beyond 100 TeV, and (5) enhance the sky survey capability, monitoring capability, and flexibility of operation (e.g., Actis et al. 2011; Funk & Hinton 2012).

In this work, we particularly focus on the nearby mini radio lobes of CORALZs (COmpact RAdio sources at Low-Redshift) which are located at the redshift of $0.005 \leqslant z \leqslant 0.16$ (Snellen et al. 2004; de Vries et al. 2009) and on the less-luminous mini lobes which will be detected by deep sensitivity observations in the future by using the next-generation radio telescope Square Kilometer Array (SKA) with its collecting area distributed over a large geographical area (see Lazio 2011 for details of its specification).

2. MODEL

First, we briefly review the model following our previous work (I11). For simplicity, we neglect the elongation of the cocoon and shell and we adopt the expanding spherical bubble model (see Figure 1). The shell width at the bubble radius $R(t)$ at the time (t) is denoted by $\delta R(t)$. The mass density of the ambient matter at $R(t)$ is defined as $\rho_{\rm a}(R(t)) = \rho_0(R(t)/R_0)^{-\alpha}$ ($0 \leqslant \alpha \leqslant 2$), where R_0 is the reference radius, $\delta R(t)$ satisfies the relation $\delta R(t) = (\hat{\gamma}_{\rm a} - 1)R(t)/[(\hat{\gamma}_{\rm a} + 1)(3 - \alpha)]$, where $\hat{\gamma}_{\rm a}$ is the specific heat ratio of the ambient matter (e.g., I11). The thin shell condition $\delta R(t) \ll R(t)$ holds when the expansion velocity has a high Mach number. We further assume that the kinetic power of the jet, $L_{\rm j}$, is constant in time. The jet kinetic energy is dissipated and deposited as the internal energy of the cocoon and shell. The internal energy drives the cocoon

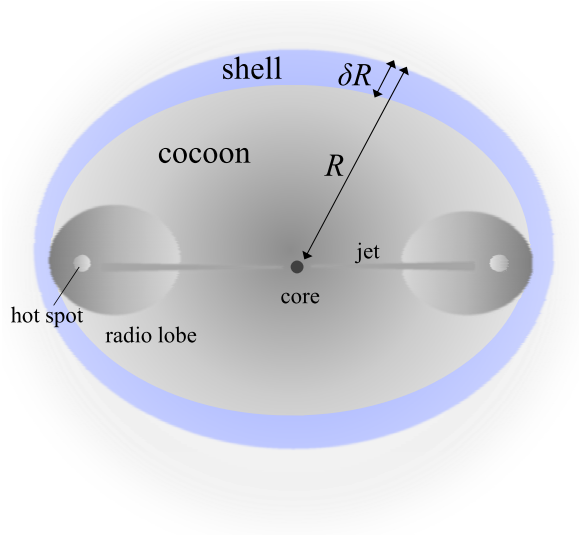

Figure 1. Schematic of relativistic jets and ambient matter interaction. The kinetic energy of the jets is dissipated via shocks at the hot spots and deposited into the cocoon with its radius R and the shell with its width δR. The cocoon is inflated by its internal energy.

(A color version of this figure is available in the online journal.)

expansion. Note that specifying a fraction of electrons/protons in the jet is irrelevant to the expansion dynamics. Solving the set of equations for the momentum and energy equations for the expanding bubble, $R(t)$ can be expressed as

$$R(t) = C R_0^{\alpha/(\alpha-5)} \left(\frac{L_{\rm j}}{\rho_0}\right)^{1/(5-\alpha)} t^{3/(5-\alpha)}, \quad (1)$$

where the coefficient C is given by $C = [(3-\alpha)(5-\alpha)^3(\hat{\gamma}_{\rm c}-1)/4\pi\{2\alpha^2+(1-18\hat{\gamma}_{\rm c})\alpha+63\hat{\gamma}_{\rm c}-28\}]^{1/(5-\alpha)}$ where $\hat{\gamma}_{\rm c}$ is the adiabatic index of the cocoon. This is identical to the well-known stellar wind model (e.g., Castor et al. 1975; Ostriker & McKee 1988). For convenience, we define the total internal energy deposited in the shell and cocoon as follows: $E_{\rm shell} = f_{\rm shell} L_{\rm j} t$, and $E_{\rm cocoon} = f_{\rm cocoon} L_{\rm j} t$, where the factors $f_{\rm shell}$ and $f_{\rm cocoon}$ can be given by $f_{\rm shell} = (18(\hat{\gamma}_{\rm c}-1)(5-\alpha)/(\hat{\gamma}_{\rm a}+1)^2[2\alpha^2+(1-18\hat{\gamma}_{\rm c})\alpha+63\hat{\gamma}_{\rm c}-28])$ and $f_{\rm cocoon} = (5-\alpha)(7-2\alpha)/[2\alpha^2+(1-18\hat{\gamma}_{\rm c})\alpha+63\hat{\gamma}_{\rm c}-28]$. Hereafter, we assume typical cases of $\hat{\gamma}_{\rm c} = 4/3$, $\hat{\gamma}_{\rm a} = 5/3$, and $\alpha = 0$. Regarding ambient matter, we set $\rho_0 = 0.1\, m_p\, {\rm cm}^{-3}$, and $R_0 = 1$ kpc, which are typical values for elliptical galaxies (see Mathews & Brighenti 2003 for review). The magnetic field strength in elliptical galaxies is ~a few μG (see Carilli & Taylor 2002 for review). Therefore, we fix the magnetic field strength in the shell to be $B_{\rm shell} = 10\,\mu$G, where we assume the shock compression ratio to be 4.

Second, we show the basic treatment of photon and electron distributions in shells and lobes. We solve the following kinetic equation describing the electron energy distribution $N_e(\gamma_e, t)$ as follows:

$$\frac{\partial N_e(\gamma_e,t)}{\partial t} = \frac{\partial}{\partial \gamma_e}[\dot{\gamma}_{\rm cool}(\gamma_e,t) N_e(\gamma_e,t)] + Q_e(\gamma_e,t), \quad (2)$$

where γ_e, $\dot{\gamma}_{\rm cool}(\gamma_e,t) = -d\gamma_e/dt = \dot{\gamma}_{\rm ad} + \dot{\gamma}_{\rm syn} + \dot{\gamma}_{\rm IC}$, and $Q_e(\gamma_e,t) \propto \gamma_e^{-p}$ are the Lorentz factor, the cooling rate via adiabatic expansions ($\dot{\gamma}_{\rm ad} = \dot{R}\gamma_e/R$), and radiative losses and the injection rate of non-thermal electrons, respectively. Regarding IC scattering, we take the Klein–Nishina cross section into account and the following seed photons are included: (1) UV photons from a standard accretion disk, (2) IR photons from a dust torus, (3) synchrotron photons from the radio lobes, (4) synchrotron photons from the shell, and (5) cosmic microwave background (CMB). As for (5), the energy density of CMB photons is sufficiently small in the present case, so we neglect it.

Third, we include the effect of absorption via $\gamma\gamma \to e^{\pm}$ interaction. VHE photons suffer from $\gamma\gamma$ absorption via interaction with various soft photons (e.g., Coppi & Aharonian 1997). Here, we include the $\gamma\gamma$ absorption due to both source-intrinsic and EBL photon fields. The $\gamma\gamma$ absorption opacity with respect to the intrinsic photons ($\tau_{\gamma\gamma}$) can be calculated by summing up all of the photons from (1) the shell, (2) the radio lobes, (3) the dusty torus, and (4) the accretion disk and we multiply the $\gamma\gamma$ absorption factor of $\exp(-\tau_{\gamma\gamma})$ with the unabsorbed flux. For simplicity, we deal with the $\gamma\gamma$ absorption effect at the first order and we neglect cascading effect. With regard to the opacity for $\gamma\gamma$ interaction between EBL and TeV photons, we adopt the model of Franceschini et al. (2008). They use the available information on extragalactic sources generating diffuse photons in the universe between far-UV and the submillimeter ranges and the opacity-corrected TeV blazars spectra are consistent with standard photon generation processes which lead to intrinsic photon indices steeper than $\Gamma_{\rm intrinsic} = 1.6$ (e.g., Aharonian et al. 2006 and references therein).

The model parameters are as follows. As for radio lobes, the fractions of non-thermal electron energy and magnetic energy are defined as $\epsilon_{\rm e,lobe}$ and $\epsilon_{\rm B,lobe}$, respectively. The spectral index, the gyro-factor, and the minimum and maximum Lorentz factors of non-thermal electrons are denoted as $p_{\rm lobe}$, $\xi_{\rm lobe}$, $\gamma_{\rm lobe,min}$, and $\gamma_{\rm lobe,max}$, respectively. As for a shell, the fraction of non-thermal electron energy to the total internal energy is defined as $\epsilon_{\rm e,shell}$. The spectral index, the gyro-factor, and the minimum and maximum Lorentz factors of non-thermal electrons are expressed as $p_{\rm shell}$, $\xi_{\rm shell}$, $\gamma_{\rm shell,min}$, and $\gamma_{\rm shell,max}$, respectively. Using the electron gyro-factor ξ_i (i = lobe or shell), the electron acceleration rate with its energy $\gamma m_e c^2$ is given by $d\gamma/dt = 3eB\dot{R}(t)^2/20\xi_i m_e c^3$. Hereafter we assume $\gamma_{\rm lobe,min} = \gamma_{\rm shell,min} = 1$. The observed range of the size $R(t) \equiv LS/2$ can be given by $5\,{\rm pc} \leqslant R(t) \leqslant 175\,{\rm pc}$, which correspond to LS/2 of the most compact and most extended sources in the CORALZ sample, i.e., J103719+433515 and J160246+524358 (de Vries et al. 2009). In this paper, we demonstrate one typical case of $R(t) = 5\,{\rm pc}$ with $z = 0.08$. Observational constraints on $L_{\rm j}$ and UV and IR luminosities at the nucleus ($L_{\rm UV}$ and $L_{\rm IR}$) are discussed in the next section.

3. OBSERVATIONAL CONSTRAINTS

Here, we show key observational constraints which restrict the model parameters.

3.1. Nucleus Luminosities: L_{UV} and L_{IR}

The luminosities $L_{\rm UV}$ and $L_{\rm IR}$ are important as the seed photons for IC scattering. In young radio sources, it is difficult to estimate them directly because they are heavily absorbed by the dusty torus (e.g., Kawakatu et al. 2009; Ostorero et al. 2010). Prior works (e.g., Snellen et al. 1999; Vink et al. 2006; Orienti et al. 2010) indicate that faint compact radio sources are generally characterized by a low level of ionization. Mack et al. (2009) observed the CORALZ sample at 250 GHz with the IRAM 30 m telescope to search for dust presence and

they indeed found dust emission in a significant fraction of the sample.

Here, we estimate $L_{\rm UV}$ and $L_{\rm IR}$ by means of observations of other compact radio sources. Kunert-Bajraszewska et al. (2010, hereafter KL10) show that low-luminosity compact radio sources' [O III]λ5007 luminosity $L_{[\rm O\,III]} \sim 10^{40}$–$10^{43}\,{\rm erg\,s^{-1}}$. Radio luminosity of KL10 sample is comparable with CORALZ one. Hence, in the case of CORALZ sample, we derive the $L_{[\rm O\,III]}$ by assuming the relation of $L_{\rm radio}$ and $L_{[\rm O\,III]}$ obtained for low-redshift radio galaxies (e.g., Buttiglione et al. 2011; Son et al. 2012), and we obtain $L_{[\rm O\,III]} \sim 10^{40}$–$10^{43}\,{\rm erg\,s^{-1}}$. Since the disk's UV emission is likely a main source for the ionization of clouds in narrow-line regions, it is reasonable to suppose that $L_{\rm UV} > L_{[\rm O\,III]}$ although it is not very clear what the re-emitting fraction is. Here, we examine the case of $L_{\rm UV} = 6\times10^{42}, 6\times10^{43}, 6\times10^{44}\,{\rm erg\,s^{-1}}$. Regarding the torus luminosity, Calderone et al. (2012) explore the fraction of torus re-emission of absorbed accretion disc radiation for about 4000 radio-quiet AGNs and they found that the torus reprocesses ∼1/3–1/2 of the accretion disk luminosity. Based on their work, we assume $L_{\rm IR} = L_{\rm UV}/2$. The IR and UV photon energy densities at $R(t)$ are given by $U_{\rm IR}(t) = L_{\rm IR}/4\pi cR(t)^2$ and $U_{\rm UV}(t) = L_{\rm UV}/4\pi cR(t)^2$, respectively.

We note that, in a few objects, a fraction of IR seed photons may arise from a dense cocoon of dust likely deposited by a merger event (e.g., Holt et al. 2009). We do not treat this case merely for simplicity.

3.2. Radio Lobe Fluxes

Optical. The CORALZ sample has been identified with bright galaxies in the Automated Plate Measuring machine catalog of the first Palomar Observatory Sky Survey, and some further identifications in the 6th Sloan Digital Sky Survey have been added, increasing the CORALZ sample in number (de Vries et al. 2009 and references therein). Since mini lobes are smaller than their host galaxies, it is hard to measure the pure emission of mini lobes.

X-ray. No X-ray observations of the CORALZ sample have been performed so far. Although the emission mechanism has not yet been confirmed (i.e., accretion disk or radio lobes), X-ray fluxes of gigahertz-peaked spectrum (GPS) and compact steep-spectrum sources have been measured by several authors recently (e.g., Tengstrand et al. 2009). Here, we regard the measured X-ray fluxes in GPS galaxies, $0.7\times10^{-14}\,{\rm erg\,cm^{-2}\,s^{-1}} \leqslant \nu F_\nu \leqslant 5.6\times10^{-13}\,{\rm erg\,cm^{-2}\,s^{-1}}$ (Guainazzi et al. 2006), as a rough upper limit of X-ray emissions from mini radio lobes and mini shells.

GeV γ-ray. Prior to the launch of *Fermi*, mini lobes were predicted to emerge as a new population of γ-ray emitters (Stawarz et al. 2008; Kino et al. 2007, 2009). With the exposure time currently accumulated by *Fermi*/LAT, however, the majority of mini lobes remain undetected except for NGC 1275 with $\nu F_\nu \sim 4\times10^{-11}\,{\rm erg\,cm^{-2}\,s^{-1}}$ (Abdo et al. 2009; Nagai et al. 2010; Suzuki et al. 2012; Aleksić et al. 2012) and possible detection of 4C+55.17 (McConville et al. 2011). We consider these detections as the upper limit of shell flux. Since the measured GeV γ flux of 4C+55.17 $\sim 1\times10^{-11}\,{\rm erg\,cm^{-2}\,s^{-1}}$ is less luminous than NGC 1275, we set it as the upper limit.

3.3. SSA Turnover Frequencies of Radio Lobes

Synchrotron self-absorption (SSA) turnover frequencies of CORALZs lobes $\nu_{\rm ssa,lobe}$ are typically less than a few hundred MHz (de Vries et al. 2009). It should be emphasized that we can constrain $L_{\rm j}\epsilon_{\rm B,lobe}$ from the $\nu_{\rm ssa,lobe}$. It is well known that the SSA turnover frequency is given by $\nu_{\rm ssa,lobe} \propto B_{\rm lobe}^{1/5} S_{\nu,\rm lobe}^{2/5} R_{\rm lobe}^{-4/5}$. Since $\nu_{\rm ssa,lobe}$, $S_{\nu,\rm lobe}$, and $R_{\rm lobe}$ are observationally determined, $B_{\rm lobe} \propto (L_{\rm j}\epsilon_{\rm B,lobe})^{1/2}$ is the only parameter where $L_{\rm j}\epsilon_{\rm B,lobe} \equiv L_{\rm poy} = 4\pi R_{\rm lobe}^2 c/3\times(B_{\rm lobe}^2/8\pi) = R_{\rm lobe}^2 cB_{\rm lobe}^2/6$, where $L_{\rm poy}$ is the Poynting power of the jet. Therefore, we stress that $L_{\rm j}\epsilon_{\rm B,lobe}$ is not a free parameter but a well-constrained quantity. With typical parameters of mini lobes, a large jet power such as $L_{\rm j} \sim 6\times10^{47}(R_{\rm lobe}/2\,{\rm pc})^2(\epsilon_{\rm B,lobe}/10^{-2})^{-1}\,{\rm erg\,s^{-1}}$ is required. The requirement of a large $L_{\rm j}\epsilon_{\rm B,lobe}$ for the SSA model has been already pointed out by several authors (Fanti et al. 1995; Stawarz et al. 2008).

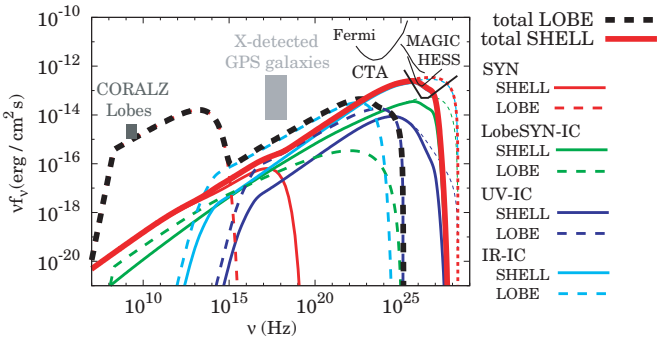

Figure 2. Mini shell and radio lobe spectra (the thick red and black curves, respectively). Here, we adopt $L_{\rm UV} = 2L_{\rm IR} = 6\times10^{43}\,{\rm erg\,s^{-1}}$, and $\epsilon_{\rm B,lobe} = 10^{-3}$. The IC components of the lobe synchrotron, UV from the accretion disk, IR from the torus, are shown in red, green, purple, blue lines, respectively. Here, we plot the radio flux of typical CORALZs (de Vries et al. 2009) and also show X-ray fluxes in GPS galaxies (Guainazzi et al. 2006) as a reference.

(A color version of this figure is available in the online journal.)

4. RESULTS

The mini shell parameters can be well constrained, since the forward shocks considered here resembles those in the well-studied supernovae remnants (SNRs). Following prior work on constraining SNRs parameters (e.g., Koyama et al. 1995; Ellison et al. 2001), here we set $\epsilon_{\rm e,shell} = 0.05$, $p_{\rm shell} = 2$, and $\xi_{\rm e,shell} = 10$. Within the observational constraint shown in Section 3.1, we demonstrate the case with $L_{\rm j} = 5\times10^{46}\,{\rm erg\,s^{-1}}$. The shell and radio lobes' kinetic luminosity is governed by $L_{\rm j}\epsilon_{\rm e,shell}$ and $L_{\rm j}\epsilon_{\rm e,lobe}$. Therefore, smaller $L_{\rm j}$ and larger $\epsilon_{\rm e,shell}$ and $\epsilon_{\rm e,lobe}$ lead to much the same results.

The mini lobe parameters are determined on the basis of the observational constraints discussed in Section 3. The radio peak flux densities of CORALZ are about ∼100–500 mJy at the peak frequency ∼1 GHz (de Vries et al. 2009) and they provide constraints $\epsilon_{\rm e,lobe}$. So as not to violate this constraint, here we set $\epsilon_{\rm e,lobe} = 0.01$. We assume $p_{\rm lobe} = 2.2$ which is suggested for relativistic shocks (e.g., Bednarz & Ostrowski 1998). A large gyro-factor $\xi_{\rm lobe} = 10^7$ is assumed due to the lack of evidence of synchrotron emission from radio lobes at optical band (e.g., Holt et al. 2007; Fanti et al. 2011). The parameter values of shell and radio lobes adopted in this work are summarized in Table 1.

In Figure 2, we show typical photon spectra from mini radio lobes and the mini shell with $L_{\rm UV} = 2L_{\rm IR} = 6\times10^{43}\,{\rm erg\,s^{-1}}$, and $\epsilon_{\rm B,lobe} = 10^{-3}$. We also plot the sensitivities adopted from the following Web sites: the *Fermi*/LAT for 1 yr integration time (http://www-glast.stanford.edu/), HESS (http://www.mpi-hd.mpg.de/hfm/HESS/), MAGIC (http://magic.mppmu.mpg.de/),

Table 1
Parameters of Shell and Radio Lobes

Parameters	Symbols	Values
Jet power	$L_{\rm j}$	5×10^{46} erg s^{-1}
Distance from core to shell	R	5 pc
Luminosity of IR emissions from dust-torus	$L_{\rm IR}$	$3 \times (10^{44}, 10^{43}, 10^{42})$ erg s^{-1}
Luminosity of UV emissions from accretion disk	$L_{\rm UV}$	$6 \times (10^{44}, 10^{43}, 10^{42})$ erg s^{-1}
Fraction of non-thermal electrons	$\epsilon_{\rm e,shell}$	0.05
Power-law index of injected electrons (shell)	$p_{\rm shell}$	2
Gyro-factor	$\xi_{\rm shell}$	10
Redshift	z	0.08
B energy fraction	$\epsilon_{\rm B,lobe}$	10^{-3}, 10^{-4}, 10^{-5}
Fraction of non-thermal electrons	$\epsilon_{\rm e,lobe}$	10^{-2}
Power-law index of injected electrons	$p_{\rm lobe}$	2.2
Gyro-factor	$\xi_{\rm lobe}$	10^7

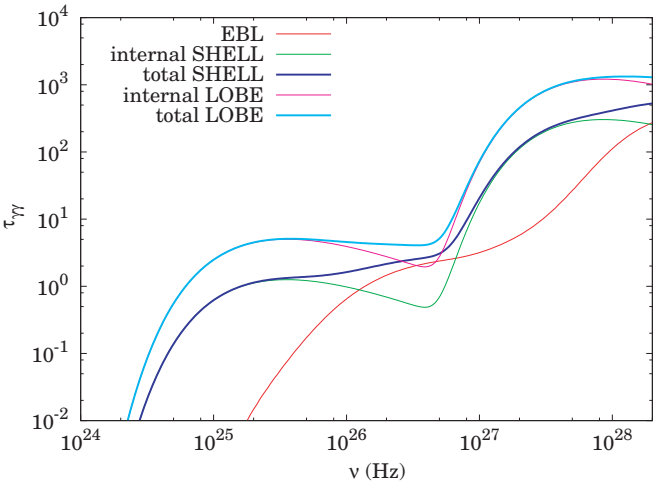

Figure 3. Opacity for $\gamma\gamma \rightarrow e^{\pm}$ corresponding to the shell spectrum in Figure 2.
(A color version of this figure is available in the online journal.)

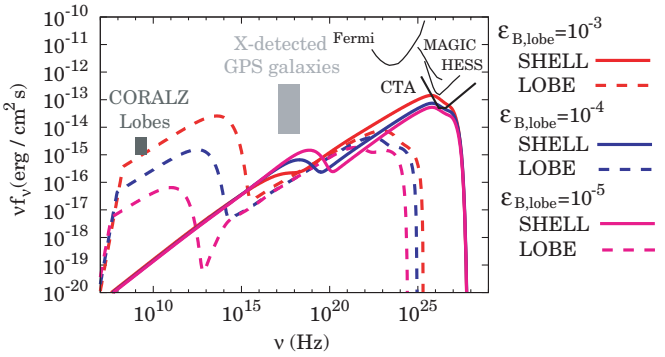

Figure 4. Same mini shell and radio lobe spectra (solid and dashed curves, respectively) but with $L_{\rm UV} = 2L_{\rm IR} = 6 \times 10^{42}$ erg s^{-1}, and $\epsilon_{\rm B,lobe} = 10^{-3}, 10^{-4}, 10^{-5}$. The seed photons for IC scattering in the mini shell are dominated by the synchrotron photons of the radio lobes.
(A color version of this figure is available in the online journal.)

and CTA (http://www.cta-observatory.org/). The thick solid and dashed lines in red and black display the total photon fluxes from the mini shell and mini radio lobe, respectively. The radio flux density and the SSA turnover frequency of the mini radio lobes are consistent with CORALZ's. Although the predicted GeV γ-ray flux appears below the *Fermi*/LAT sensitivity curve, the distinctive double-bump structure in the IC spectrum is found reflecting UV and IR emission bumps at the core. As already shown in I11, synchrotron emission from the mini shell is very dim. It explains well the lack of detection of shells so far. On the other hand, bright IC emission is expected in the VHE range and it will be detectable by CTA. In Figure 2, the mini shell spectrum without the EBL absorption effect is shown in the thin dotted curve. From this, we see that the EBL absorption is effective above a few 10^{26} Hz. In Figure 3, we show the corresponding optical depth for $\gamma\gamma$ absorption $\tau_{\gamma\gamma}$ plotted versus the corresponding high-energy photon frequency ν. At the frequency below $\sim 10^{26}$ Hz, the number density of target photons from radio lobes is larger than that from the shell; therefore, the photons from the lobe dominate the absorption opacity. Since the contribution of the shell's synchrotron photons is sufficiently small as seed photons of IC and $\gamma\gamma$ absorption, we neglect them to save computational cost.

In Figure 4, we present predicted spectra with smaller $L_{\rm UV} = 2L_{\rm IR} = 6 \times 10^{42}$ erg s^{-1}, and $\epsilon_{\rm B,lobe} = 10^{-3}, 10^{-4}, 10^{-5}$. Here, $\epsilon_{\rm B,lobe}$ has been carefully chosen not to exceed the observed radio lobe luminosities, i.e., $\sim$(1–5) $\times 10^{-15}$ erg s^{-1} cm^{-2} at $\sim$1 GHz. If $L_{\rm UV}$ becomes smaller, then the lobe becomes synchrotron-dominated and the synchrotron luminosity becomes larger even for the same $\epsilon_{\rm B,lobe}$. Hence, the radio flux tends to be overproduced. We therefore search parameter values according to $\epsilon_{\rm B,lobe} \propto L_{\rm UV}$ so as not to overproduce the lobe radio flux. Overall features of shell spectra are similar to the case in Figure 2, and the mini shell spectrum is detectable by CTA. However, the radio lobe IC emission is less luminous than the ones in Figure 2 at GeV band simply because of smaller $L_{\rm UV} = 2L_{\rm IR}$. Seed photons for IC scattering in the mini shell are dominated by the synchrotron photons from the lobes. In the IC-dominated regime, the peak luminosity of IC emission is proportional only to the $L_{\rm j}\epsilon_{\rm e,shell}$ (see Equation (24) in I11) and it only has a weak dependence on $L_{\rm UV}$ and $L_{\rm IR}$. The shell luminosity at the TeV range becomes slightly brighter as the synchrotron emission of the radio lobes increases. Therefore, our prediction of emission spectra does not strongly depend on the choice of $L_{\rm UV}$ and $L_{\rm IR}$.

In Figure 5, we further present predicted spectra with larger $L_{\rm UV} = 2L_{\rm IR} = 6 \times 10^{44}$ erg s^{-1}, and $\epsilon_{\rm B,lobe} = 10^{-3}, 10^{-4}, 10^{-5}$. Overall features of shell and lobe spectra are similar to the cases in Figures 1 and 2 the mini shell spectrum is detectable by CTA. In this case, seed photons for IC scattering are dominated by the emission of the nucleus $L_{\rm UV} = 2L_{\rm IR}$. Therefore, the shell IC luminosity in the TeV band remains constant for various $\epsilon_{\rm B,lobe}$. Interestingly, the intrinsic absorption in the mini shell produces the dip around $\sim 10^{25}$ Hz.

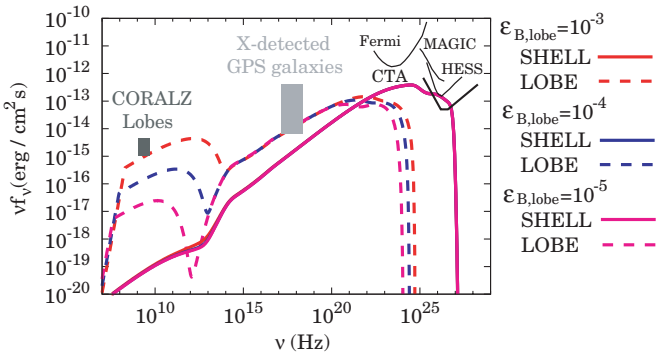

Figure 5. Same mini shell and radio lobe spectra (solid and dashed curves, respectively) but with $L_{\rm UV} = 2L_{\rm IR} = 6 \times 10^{44}\,{\rm erg\,s^{-1}}$, and $\epsilon_{\rm B,lobe} = 10^{-3}, 10^{-4}, 10^{-5}$. The seed photons for IC scattering in the mini shell are dominated by the core UV and IR photons.

(A color version of this figure is available in the online journal.)

5. SUMMARY AND DISCUSSIONS

In the present work, we have studied non-thermal emissions from mini shells surrounding low-luminosity, mini radio lobes. Predicted synchrotron emissions from mini shells are very faint due to their weak magnetic field. On the other hand, IC scattering in the mini shell is significantly effective since the energy densities of soft photons from AGN nucleus and synchrotron photons from the radio lobe are large. As a result, the IC emission from the shell overwhelms the emission from the radio lobe in VHE γ-ray range. We find that the non-thermal emission from the mini shells can be detectable by CTA and they become a potential new class of VHE γ-ray emitters.

Among FIRST survey sources (White et al. 1997), the candidate selection of CORALZ for further very long baseline interferometry (VLBI) confirmation had been done with the criteria of the flux density >100 mJy at 1.4 GHz and the angular size <2″ (de Vries et al. 2009). Hence, a straightforward way to increase the number of lower luminosity radio lobes is to conduct further VLBI survey with a flux density threshold lower than 100 mJy among FIRST survey sources. Then, more lower luminosity lobes will be found. Another promising way to find less luminous mini radio lobes is a deep survey with the next-generation radio telescope SKA with its collecting area distributed over a large geographical area. Such deep observations will significantly increase the number of radio-dark mini shells, a new class of VHE γ-ray emitters, which can be potentially detected by CTA.

We thank the referee for suggestions to improve the paper. This work is partially supported by the Grant-in-Aid for Scientific Research, KAKENHI 24540240 (M.K.) from the Japan Society for the Promotion of Science (JSPS) and by Research Activity Start-up 2284007 (N.K.) from the Ministry of Education, Culture, Sports, Science, and Technology (MEXT). Part of this work was done with the contribution of the Italian Ministry of Foreign Affairs and Research for the collaboration project between Italy and Japan.

REFERENCES

Abdo, A. A., Ackermann, M., Ajello, M., et al. 2009, ApJ, 699, 31
Actis, M., Agnetta, G., Aharonian, F., et al. 2011, ExA, 32, 193
Aharonian, F., Akhperjanian, A. G., Bazer-Bachi, A. R., et al. 2006, Natur, 440, 1018
Aleksić, J., Alvarez, E. A., Antonelli, L. A., et al. 2012, A&A, 539, L2
Bednarz, J., & Ostrowski, M. 1998, PhRvL, 80, 3911
Buttiglione, S., Capetti, A., Celotti, A., et al. 2011, A&A, 525, A28
Calderone, G., Sbarrato, T., & Ghisellini, G. 2012, MNRAS, 425, L41
Carilli, C. L., Perley, R. A., & Dreher, J. H. 1988, ApJL, 334, L73
Carilli, C. L., & Taylor, G. B. 2002, ARA&A, 40, 319
Castor, J., McCray, R., & Weaver, R. 1975, ApJL, 200, L107
Coppi, P. S., & Aharonian, F. A. 1997, ApJL, 487, L9
Croston, J. H., Kraft, R. P., & Hardcastle, M. J. 2007, ApJ, 660, 191
Croston, J. H., Kraft, R. P., Hardcastle, M. J., et al. 2009, MNRAS, 395, 1999
de Vries, N., Snellen, I. A. G., Schilizzi, R. T., Mack, K.-H., & Kaiser, C. R. 2009, A&A, 498, 641
Ellison, D. C., Slane, P., & Gaensler, B. M. 2001, ApJ, 563, 191
Fanti, C., Fanti, R., Dallacasa, D., et al. 1995, A&A, 302, 317
Fanti, C., Fanti, R., Zanichelli, A., Dallacasa, D., & Stanghellini, C. 2011, A&A, 528, A110
Franceschini, A., Rodighiero, G., & Vaccari, M. 2008, A&A, 487, 837
Funk, S., & Hinton, J. 2012, APh, in press (arXiv:1205.0832)
Guainazzi, M., Siemiginowska, A., Stanghellini, C., et al. 2006, A&A, 446, 87
Holt, J., Tadhunter, C. N., González Delgado, R. M., et al. 2007, MNRAS, 381, 611
Holt, J., Tadhunter, C. N., & Morganti, R. 2009, MNRAS, 400, 589
Ito, H., Kino, M., Kawakatu, N., & Yamada, S. 2011, ApJ, 730, 120 (I11)
Kawakatu, N., Nagao, T., & Woo, J.-H. 2009, ApJ, 693, 1686
Kino, M., Ito, H., Kawakatu, N., & Nagai, H. 2009, MNRAS, 395, L43
Kino, M., Kawakatu, N., & Ito, H. 2007, MNRAS, 376, 1630
Koyama, K., Petre, R., Gotthelf, E. V., et al. 1995, Natur, 378, 255
Kunert-Bajraszewska, M., & Labiano, A. 2010, MNRAS, 408, 2279
Lazio, J. 2011, on behalf of Science Working Group 2011, The Square Kilometre Array Design Reference Mission: SKA Phase I (SCI-020.010.020-DRM-002)
Mack, K.-H., Snellen, I. A. G., Schilizzi, R. T., & de Vries, N. 2009, AN, 330, 217
Mathews, W. G., & Brighenti, F. 2003, ARA&A, 41, 191
McConville, W., Ostorero, L., Moderski, R., et al. 2011, ApJ, 738, 148
Nagai, H., Suzuki, K., Asada, K., et al. 2010, PASJ, 62, L11
Ostorero, L., Moderski, R., Stawarz, L., et al. 2010, ApJ, 715, 1071
Ostriker, J. P., & McKee, C. F. 1988, RvMP, 60, 1
Orienti, M., Dallacasa, D., & Stanghellini, C. 2010, MNRAS, 408, 1075
Snellen, I. A. G., Mack, K.-H., Schilizzi, R. T., & Tschager, W. 2004, MNRAS, 348, 227
Snellen, I. A. G., Schilizzi, R. T., Bremer, M. N., et al. 1999, MNRAS, 307, 149
Son, D., Woo, J.-H., Kim, S. C., et al. 2012, ApJ, 757, 140
Stawarz, Ł., Ostorero, L., Begelman, M. C., et al. 2008, ApJ, 680, 911
Su, M., Slatyer, T. R., & Finkbeiner, D. P. 2010, ApJ, 724, 1044
Suzuki, K., Nagai, H., Kino, M., et al. 2012, ApJ, 746, 140
Tengstrand, O., Guainazzi, M., Siemiginowska, A., et al. 2009, A&A, 501, 89
Vink, J., Snellen, I., Mack, K.-H., & Schilizzi, R. 2006, MNRAS, 367, 928
White, R. L., Becker, R. H., Helfand, D. J., & Gregg, M. D. 1997, ApJ, 475, 479